J Mater Sci (2016) 51:10429–10441

Ferromagnetic properties of barium titanate ceramics doped with cobalt, iron, and nickel

H. T. Langhammer[1,*], T. Müller[1], T. Walther[1], R. Böttcher[2], D. Hesse[3], E. Pippel[3], and S. G. Ebbinghaus[1]

[1] *Institut für Chemie, Martin-Luther-Universität Halle-Wittenberg, Kurt-Mothes-Straße 2, 06120 Halle (Saale), Germany*
[2] *Fakultät für Physik und Geowissenschaften, Universität Leipzig, Linnéstraße 5, 04103 Leipzig, Germany*
[3] *Max-Planck-Institut für Mikrostrukturphysik Halle, Weinberg 2, 06120 Halle (Saale), Germany*

Received: 8 June 2016
Accepted: 26 July 2016
Published online: 4 August 2016

ABSTRACT

The influence of annealing in strongly reducing atmosphere on the magnetic properties of hexagonal $BaTiO_3 + 0.04\ BaO + x/2\ Co_2O_3$ ($0.0025 \leq x \leq 0.10$) ceramics was investigated. The samples air-sintered at 1673 K were subsequently tempered at 1473 K in H_2/Ar stream. While the as-sintered samples exclusively exhibit paramagnetic behavior, the annealed samples show distinct saturation in the field dependence of the magnetization at 300 K measured in the range between −90 and 90 kOe. Besides, the field dependence of the magnetization is hysteretic with coercive fields in the order of 100 Oe. Both properties point to ferromagnetic regions which were identified as precipitations of metallic cobalt by TEM and EDX. The cobalt precipitations were exclusively found in tetragonal grains which were completely Co-free outside the precipitations. Obviously, these tetragonal grains were formed during the annealing process when the Co content of the formerly hexagonal grains was concentrated into metallic Co particles by diffusion processes. Hence, the Co-free matrix of the grains transformed into the cubic phase which is the equilibrium phase of undoped $BaTiO_3$ at the annealing temperature 1473 K and during cooling to room temperature into tetragonal phase. The size of the metallic precipitations ranges from about 20 to 100 nm. A reduction both of the annealing temperature to 1373 K and of the annealing time from 120 to 30 min did not change the minimum particle size, but now, the very rare precipitations only occurred at triple points or grain boundaries. EPR measurements confirmed the occurrence of the ferromagnetic precipitations. While at 300 K, the as-sintered samples did not show any Co EPR signal, the annealing in strongly reducing atmosphere caused a strong and broad line which is attributed to the ferromagnetic resonance signal of the Co precipitations. The investigations were extended for the dopants, iron or nickel, with a nominal sample composition of $BaTiO_3 + 0.04\ BaO + 0.01\ Fe_2O_3$ or 0.02 NiO, respectively. The field dependence of the magnetization as well as the EPR spectra showed similar results compared to the case of Co-doped samples. Hence, also in Fe- or Ni-doped $BaTiO_3$ ceramics, ferromagnetic properties are caused by annealing in strongly reducing atmosphere.

Address correspondence to E-mail: hans.langhammer@physik.uni-halle.de

DOI 10.1007/s10853-016-0263-3

Introduction

Multiferroics are a class of solids in which ferroelectric and magnetic orders coexist. These materials have the potential ability to couple electric polarization and magnetization and provide an additional degree of freedom in device design. Therefore, they are subject of intense investigations. However, multiferroics are quite rare in nature, particularly at room temperature (RT) and above [1, 2]. Thus, a considerable number of studies have been performed on the fabrication of multiferroic materials in recent years. Barium titanate ($BaTiO_3$), a ferroelectric oxide with perovskite structure, has become one of the promising systems. At present, much interest is focused on the realization of ferromagnetism in $BaTiO_3$ by doping with paramagnetic (PM) ions of the 3d group. Due to their strong resemblance to the titanium ion, most of the 3d transition metals can be easily doped into $BaTiO_3$ and act as substitutes for titanium [3, 4]. So far, ferromagnetic (FM) ordering has been achieved in Co- [5, 6], Mn- [5], and Fe-doped [6–16] $BaTiO_3$ systems (single crystals [5, 6, 11, 13, 14], thin films [7–9], and ceramics [10, 12, 15, 16]). While the vast majority of published works concern Fe-doped $BaTiO_3$, there are only a few reports on ferromagnetism with other 3d dopants, but, e.g., no report is found in which Ni-doping would cause ferromagnetism. Often, the researchers searched for the so-called ferromagnetism in diluted magnetic oxides (DMO) [11, 13–16], but it seems that ferromagnetism can also be caused by metallic precipitations formed during the preparation of the samples. Thus, Chakraborty et al. [13] reported on dilute magnetism in Fe-doped $BaTiO_3$ single crystals, but later they proposed that metallic Fe clusters formed inside the $BaTiO_3$ lattice were responsible for the FM behavior of the specimens [14]. Among the different preparation methods for achieving FM material, only two different procedures are to be mentioned here. Khalitov et al. [6] implanted $BaTiO_3$ single crystals by Co and Fe ions, respectively. Depending on the strength of the ion fluence, they achieved metallic particles inside the samples with different particle sizes. These particles caused either superparamagnetic (SPM) or FM properties. The critical particle size below which SPM behavior occurs (and above which FM properties occur), is found to be 5.0 nm for Co implantation and 6.5 nm for Fe implantation. Another way to produce FM behavior is the post-annealing of ceramic samples either in vacuum [10] or in pure oxygen at 10^5 Pa [10, 15, 16]. However, for specimens produced in this way, it could be also assumed here that metallic precipitations of the dopant (formed by the heat treatment) cause the ferromagnetism of the samples.

During our recent investigations of the PM defect properties of Co incorporated at Ti sites in hexagonal $BaTiO_3$ ceramics in the doping range of 0.1–2.0 mol% Co [17], we tried to vary the Co valence state by annealing in ambient atmospheres with various oxygen partial pressures (pO_2) from 10^5 Pa (pure oxygen) to $pO_2 < 10^{-10}$ Pa (mixtures of H_2/Ar). While the samples annealed under $pO_2 \approx 0.1$ Pa (Ar, 5 N) remained completely PM, the treatment in H_2/Ar caused a distinct saturation of the magnetization field dependence pointing to FM or SPM properties of the samples.

To the best of our knowledge, there are no publications of systematic investigations on achieving ferromagnetism or superparamagnetism in Co-doped $BaTiO_3$ ceramics by heat treatment in highly reducing atmosphere.

Thus, the aim of this paper is a detailed investigation of the cause and the properties of the FM/SPM behavior of Co-doped $BaTiO_3$ ceramics in the doping range up to 10 mol%. These investigations include (1) X-ray diffraction (XRD) for the macroscopic phase composition, (2) measurement of the field dependence of the magnetization, (3) the use of transmission electron microscopy (TEM) partly combined with energy-dispersive X-ray microanalysis (EDX) for the localization and chemical identification of the FM/SPM particles, and (4) electron paramagnetic resonance (EPR) measurements for the characterization of the local defect properties. In addition, we present investigations of hexagonal $BaTiO_3$ ceramics doped with 2 mol% Fe or Ni, respectively, treated under the same reducing conditions as for the Co-doped samples to verify the FM/SPM properties also for the other two ferromagnetic 3d transition metals, Fe and Ni.

Experimental procedure

Ceramic powders with the nominal composition $BaTiO_3 + 0.04\ BaO + x/2\ Co_2O_3$ ($0.0025 \le x \le 0.10$) and $BaTiO_3 + 0.04\ BaO + 0.01\ Fe_2O_3$ or 0.02 NiO were prepared by the conventional mixed-oxide

powder technique.[1] After mixing (agate balls, water) and calcining (1373 K, 2 h) of $BaCO_3$ (Solvay, VL600, <0.1 mol% Sr) and TiO_2 (Merck, No. 808), appropriate amounts of either Co_2O_3 (Apolda-Chemie, p.a.) or Fe_2O_3 (Merck, p.a.) or NiO (Berlin-Chemie, p.a.) were added to the $BaTiO_3$ powder. Then it was fine-milled (agate balls, 2-propanole) and densified into disks with a diameter of 6 mm and a height of nearly 3 mm. The samples were sintered in air at 1673 K for 1 h (heating rate 10 K/min). After the sintering, the samples were annealed in a stream of H_2/Ar (20/20 ml/min) at 1473 K for 120 min (regime T0). The Co-doped samples with a nominal Co concentration of 1.5 mol% were annealed under three different temperature/time regimes. Apart from regime T0, some sintered samples were annealed at the same temperature of 1473 K with reduced soaking time of 30 min (T1) or at reduced temperature/time of 1373 K for 30 min (T2).

The microstructure of the resulting ceramics was examined by optical microscopy of cut planes through the sample center. The mean grain sizes were roughly estimated from the two-dimensional grain areas in the cut plane. The overall phase composition was determined quantitatively by XRD of pulverized samples (STADI MP diffractometer, STOE, Germany using Co-$K_{\alpha 1}$ radiation equipped with a Ge(111) monochromator and image plate detector). The percentage of tetragonal phase c_{tg} was determined using the following equation: $c_{tg} = \frac{a-b\cdot R}{c\cdot R-d}$ considering two different peak height ratios R $(111)_{tetragonal}/(103)_{hexagonal}$ and $(200)_{tetragonal}/(103)_{hexagonal}$ and averaging both results. Parameters a, b, c, d were determined by calibration with well-defined mixtures of pure tetragonal and hexagonal barium titanates. The percentage phase composition of the samples is given as mass percent throughout the article.

Magnetic measurements were carried out using the ACMS magnetometer option of a PPMS 9 (Quantum Design). The field dependence of the magnetic moment was measured at 300 K with magnetic field cycling between 90 and −90 kOe. The obtained magnetic moments were corrected for the magnetic moment of the sample holder and with respect to the magnetic contribution of the $BaTiO_3$ matrix.

Transmission electron microscopy (TEM) investigations were performed using a Philips CM20T electron microscope with energy of the primary electrons of 200 keV, after thinning the samples by standard methods involving mechanical polishing and dimpling as well as argon ion beam thinning. For performing scanning transmission electron microscopy (STEM) and energy-dispersive X-ray (EDX) elemental analyses, a FEI TITAN 80-300 high-performance electron microscope was used, operating at 300 keV and equipped with a probe Cs-corrector and an EDAX X-ray detector. This allows for the elemental analysis with a spatial resolution in the order of a few tenths of a nanometer.

EPR measurements of well-crushed ceramic samples were carried out on an X-band ELEXYS E580 spectrometer equipped with an Oxford Instruments cryostat ESR 910 and a universal ER4102ST cavity (TE_{102} mode) with a grid (50 % transmittance) for optical excitation. For experiments in the Q-band, we used a Bruker EMX device with a cylindrical cavity ER 5106 QT (TE_{012}) and an Oxford Instruments cryostat CF 935.

Results and discussion

Co-doped samples

XRD and microstructure

Figure 1 shows the percentage of tetragonal phase at room temperature as a function of the nominal Co concentration of air-sintered samples as well as of samples which were additionally annealed in strongly reducing atmosphere (H_2/Ar stream, 1473 K, 120 min, called annealing T0). In the whole Co-doping range investigated, exclusively tetragonal and hexagonal $BaTiO_3$ phases were found within the detection limit of roughly 5 wt%. Thus, in Fig. 1, the remaining percentage corresponds to the hexagonal phase. For the air-sintered samples, the hexagonal phase starts to occur at about $x = 0.001$ [17] and for $x > 0.005$ the samples are completely hexagonal.[2] The reducing treatment of the samples causes a small, but remarkable change of the phase composition. Whereas for $x \leq 0.005$ the reducing annealing

[1] The slight Ba-excess supports the preferred incorporation of Co on Ti sites in the air-sintered samples [17].

[2] The influence of Co and other 3d transition elements on the stabilization of the hexagonal phase of $BaTiO_3$ at room temperature is not yet fully understood [20–22].

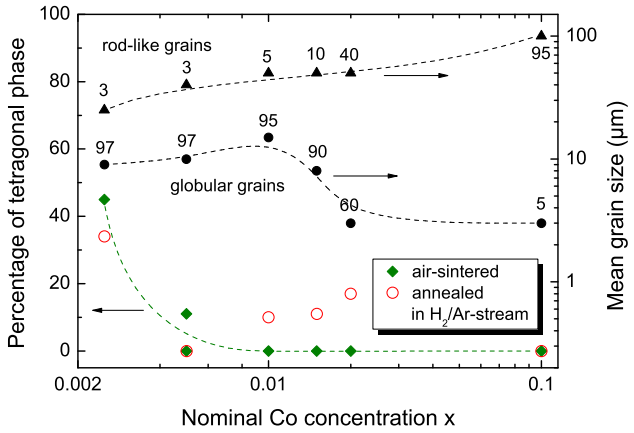

Figure 1 Room-temperature fraction of tetragonal phase for Co-doped $BaTiO_3$ sintered in air at 1673 K as well as subsequently annealed in H_2/Ar stream at 1473 K as a function of the nominal Co concentration. The accuracy of the percentage data is not better than 10 %. In addition, the average grain sizes of the air-sintered samples are shown. *Hollow/solid* symbols indicate different fractions of a bimodal microstructure. For the rod-like fraction, the approximate length of the rods is used. Numbers at the data points denote the percentage of these grain fractions.

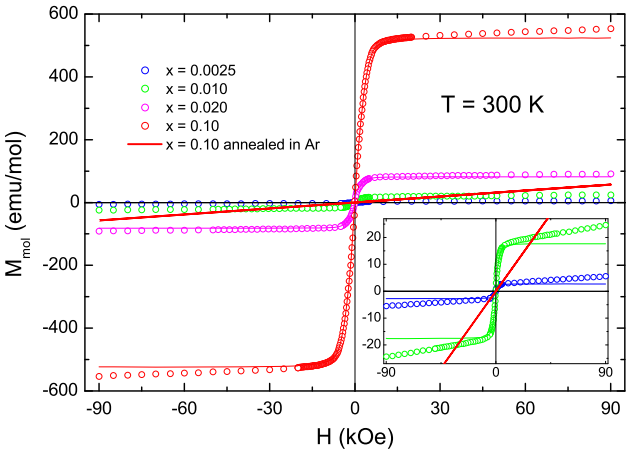

Figure 2 Room-temperature magnetic field dependence of the molar magnetization of Co-doped $BaTiO_3$ ceramics sintered in air at 1673 K and subsequently annealed in H_2/Ar stream at 1473 K for nominal Co concentrations $x = 0.0025$, 0.010, 0.020, and 0.010.

increases the percentage of the hexagonal phase, for larger Co concentrations $x \geq 0.01$ it causes a retransformation into the tetragonal phase with a maximum percentage of 17 %. Only the specimens with the highest Co concentration $x = 0.10$ remain completely hexagonal.

The microstructure data of the Co-doped samples are also depicted in Fig. 1. A bimodal grain size distribution is observed, which is characterized by small globular grains and rod-like grains with large aspect ratios which are typical for hexagonal $BaTiO_3$ ceramics with its strongly anisotropic grain growth [18, 19]. In contrast to Mn-, Cu-, and Cr-doped h-$BaTiO_3$ [20–22], the amount of these rod-like grains (of Co-doped samples) does not reflect the portion of hexagonal phase determined by XRD. Only at $x = 0.10$, the majority of the grains exhibit the typical rod-like shape. The reducing treatment does not change the microstructure of the ceramics.

Magnetic measurements

The air-sintered Co-doped samples exhibit exclusively PM behavior (superimposed by the weak diamagnetism of the $BaTiO_3$ matrix), which is caused by the PM defect Co^{2+} incorporated at Ti sites. Extensive investigations of the PM Co-doped $BaTiO_3$ ceramics were published recently [17]. The annealing treatment in strongly reducing atmosphere according to the regime T0 drastically changes the magnetic properties of the samples. Figure 2 shows the magnetic field (H) dependence of the molar magnetization (M_{mol}, related to the mole number of $BaTiO_3$) of the Co-doped samples ($0.0025 \leq x \leq 0.10$) in the field range of ±90 kOe measured at 300 K. All samples exhibit distinct saturation behavior of the magnetization which is superimposed by a PM contribution. The latter is clearly caused by isolated PM Co^{2+} ions at Ti sites still occurring in the ceramic grains after the reducing treatment. It has to be emphasized that the annealing in Ar atmosphere (oxygen partial pressure ≈ 0.1 Pa) with the same temperature schedule (which acts as a reducing treatment milder than H_2/Ar) does not cause such a saturation of the magnetization, i.e., the samples remain completely paramagnetic, which is shown in Fig. 2 for $x = 0.10$ exemplarily. The S-shaped $M_{mol}(H)$ curves point to either FM or SPM properties of metallic particles which were formed by the reduction of Co^{2+} and Co^{3+} ions (occurring in the air-sintered samples [17]) to elemental Co atoms. Because of the observed curve shapes, the Co atoms must have formed metallic clusters. Whether the particles show FM or SPM behavior depends on the cluster size. Generally, if the size of the particles exceeds about 10 nm, they become ferromagnetic and form different, room-temperature stable magnetic domains. A distinctive feature for SPM is the vanishing of a hysteretic $M_{mol}(H)$ behavior

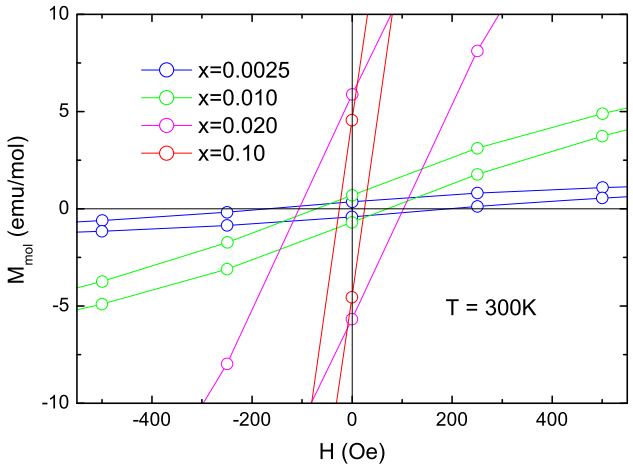

Figure 3 Enlarged region of ±500 Oe of Fig. 2 to reveal the magnetic hysteresis behavior of the samples.

above a certain blocking temperature [23]. The measuring temperature of 300 K is well above typical blocking temperatures for SPM cobalt, thus, no hysteresis should be detectable for samples showing exclusive SPM. The enlarged field range of ±500 Oe of Fig. 2 (shown in Fig. 3) clearly reveals the hysteretic properties of all samples investigated ($0.0025 \leq x \leq 0.10$). Hence, all samples exhibit FM behavior, but coexisting SPM particles cannot be excluded at this state of the investigation. The remanent magnetizations M_{rem} and coercive fields H_{coerc} are listed in Table 1 together with the percentages of M_{rem} related to the saturation magnetizations M_{sat}. The latter were determined by subtraction of the PM, linear field-dependent magnetization from the total magnetization. The resulting curves are shown in Fig. 2 (solid lines). Table 1 also includes the ratio between the PM contribution at 90 kOe and the FM/SPM-caused M_{sat} and finally the mass percentage of the FM/SPM particles related to the total amount of weighed Co-dopant. The total mass of the FM/SPM particles was calculated by the saturation magnetization and the magneton number of Co atoms of 1.72 [24]. The given magneton number is related to 0 K. Since the saturation magnetization of Co only changes by 0.4 % between 0 and 300 K [24], the resulting mass error can be ignored. The relative quantities of Table 1 are shown in Fig. 4. The relative remanent magnetization and the relative PM part of M_{mol} are decreasing with the increasing Co concentration. The trend of the PM contribution corresponds well with the development of FM/SPM particles, since the mass percentage of these particles increases with the increasing Co concentration. At $x = 0.10$, more than half of the weighed Co dopant is in the metallic phase.

To check the occurrence of small SPM particles, the commonly used simple model function for the field dependence of the magnetization (assuming uniform particle size and equal magnetic properties of all particles),

$$M(H) = M_{sat} L\left(\frac{\mu_0 H m_{mag}}{k_B T}\right) \quad (1)$$

was applied, see e.g. [25]. $L(x) = \coth(x) - x^{-1}$ is the Langevin function, m_{mag} the magnetic moment of a single SPM particle, μ_0 the vacuum permeability and k_B the Boltzmann constant. Neglecting the small coercive field <200 Oe, the $M_{mol}(H)$ curves of all samples could be satisfyingly fitted by Eq. 1. Starting from the values of M_{sat}, of the fit parameter m_{mag} and of the total mass of SPM particles, the volume of the particles can be estimated. Taking the upper mass limit as the total mass of metallic particles (see Table 1), i.e., all particles are SPM and assuming spherical particles, the estimated particle size of the

Table 1 Extracted data from the magnetic field dependence of the molar magnetization of Co-doped $BaTiO_3$ ceramics (Fig. 2) and of Fe-, Ni-doped $BaTiO_3$ ceramics (Fig. 11)

Dopant conc. (x)	H_{coerc} (Oe)	M_{rem} (emu/mol)	M_{sat} (emu/mol)	M_{rem}/M_{sat} (%)	M_{PM}/M_{sat} (%)	$M_{FM}/m_{weighed}$ (%)
Co 0.0025	182	0.39	2.72	14	104	11
Co 0.010	71	0.70	17.6	4.0	39	18
Co 0.020	104	5.8	82.2	7.1	11	43
Co 0.100	25	4.6	524	0.9	5.5	54
Fe 0.020	52	0.75	51.6	1.5	31	21
Ni 0.020	45	1.4	36.2	3.9	6.4	54

M_{PM} paramagnetic part of the molar magnetization at 90 kOe, m_{FM} total mass of metallic (Co, Fe, Ni) particles in the samples, $m_{weighed}$ initially weighed dopant amount

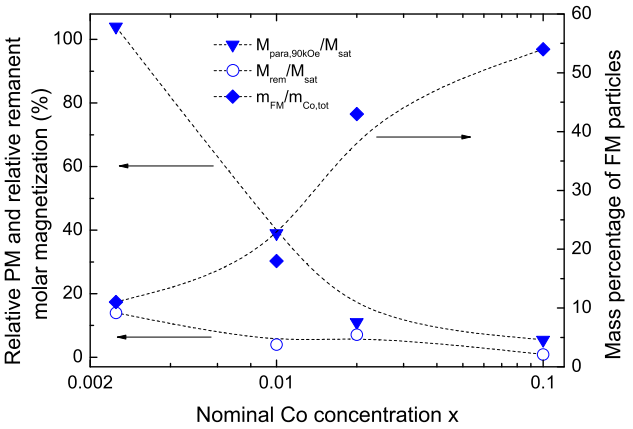

Figure 4 Relative remanent molar magnetization, relative PM part of the magnetization at 90 kOe, and percentage of the metallic Co particles with respect to the total Co weighing dependent on the nominal Co concentration.

sample with $x = 0.02$ is about 4.2 nm as an upper limit. The estimation of the maximum SPM particle size of all other samples resulted in values of the same order. Therefore, this fitting approach is not adequate. Hence, to answer the question about the coexistence of small SPM particles, investigations of transmission electron microscopy (TEM), partly combined with energy-dispersive X-ray microanalysis (EDX) were performed to locate the metallic Co particles in the sample's interior and to determine their size distribution.

TEM and EDX

The investigations by electron microscopy were performed with samples of a cobalt concentration $x = 0.015$, which is representative for the specimens up to $x = 0.02$. The sintering and annealing (H_2/Ar) conditions of the specimens correspond to the samples presented in the previous chapters.

TEM images were taken for a large number of different grains to ensure a sufficiently detailed overview of the sample. It was proven that the majority of the grains do not contain any precipitations of Co, which can be detected as dark globular regions since their atomic number is higher than the mean atomic number of the surrounding $BaTiO_3$ matrix. Dark precipitations, being probably the searched Co particles, could be detected only in relatively few grains, shown in Fig. 5 as examples for different grains and magnifications. The particle size varies between 30 and 100 nm with a mean of 50–60 nm. Interestingly, all these grains exhibit a domain pattern, whereas the grains without precipitations do not show such patterns. Hence, it can be supposed that the few grains with domains represent tetragonal, i.e., ferroelectric $BaTiO_3$, whereas the precipitation-free grains are in the hexagonal phase. Electron diffraction patterns measured at selected grains confirm that assumption. This finding corresponds very well with the overall phase composition determined by XRD, which shows a ratio between the hexagonal and tetragonal phases of about 90:10 (see Fig. 1). To identify the precipitations as Co particles further measurements were performed with the analytical STEM TITAN 80–300 provided with an EDX detector. Figure 6a shows the results inside a tetragonal grain. Whereas the precipitation (measuring point 1) is clearly identified as a particle of metallic Co (Co-rich Ba and/or Ti containing compounds are excluded because of the measured FM/SPM properties), the tetragonal matrix (measuring point 2) is completely Co-free (within the detection limit). In Fig. 6b, a region near the grain boundary between a hexagonal and a tetragonal grain is shown. While the findings in the tetragonal grain confirm the results in Fig. 6a (measuring points 1 and 2), the Co concentration in the hexagonal grain (measuring point 3) amounts to about 0.9 mol% ($x = 0.009$). Since

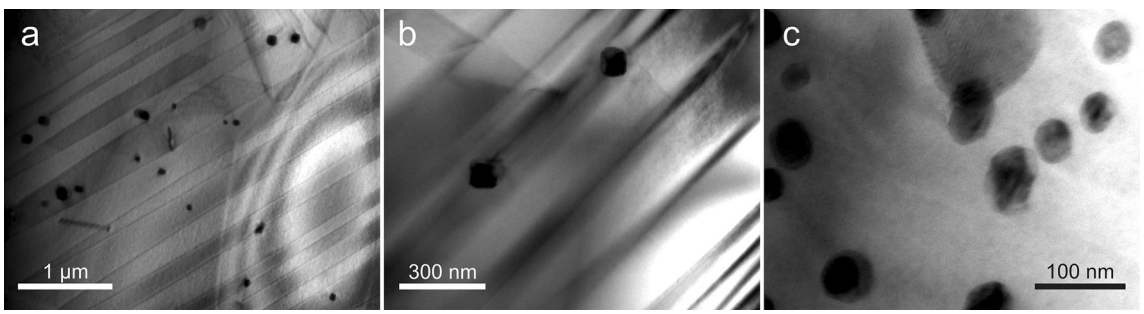

Figure 5 TEM diffraction contrast images of Co particles in different tetragonal $BaTiO_3$ grains ($x = 0.015$, annealing regime T0) at different magnifications. The stripes are ferroelectric 90° domains.

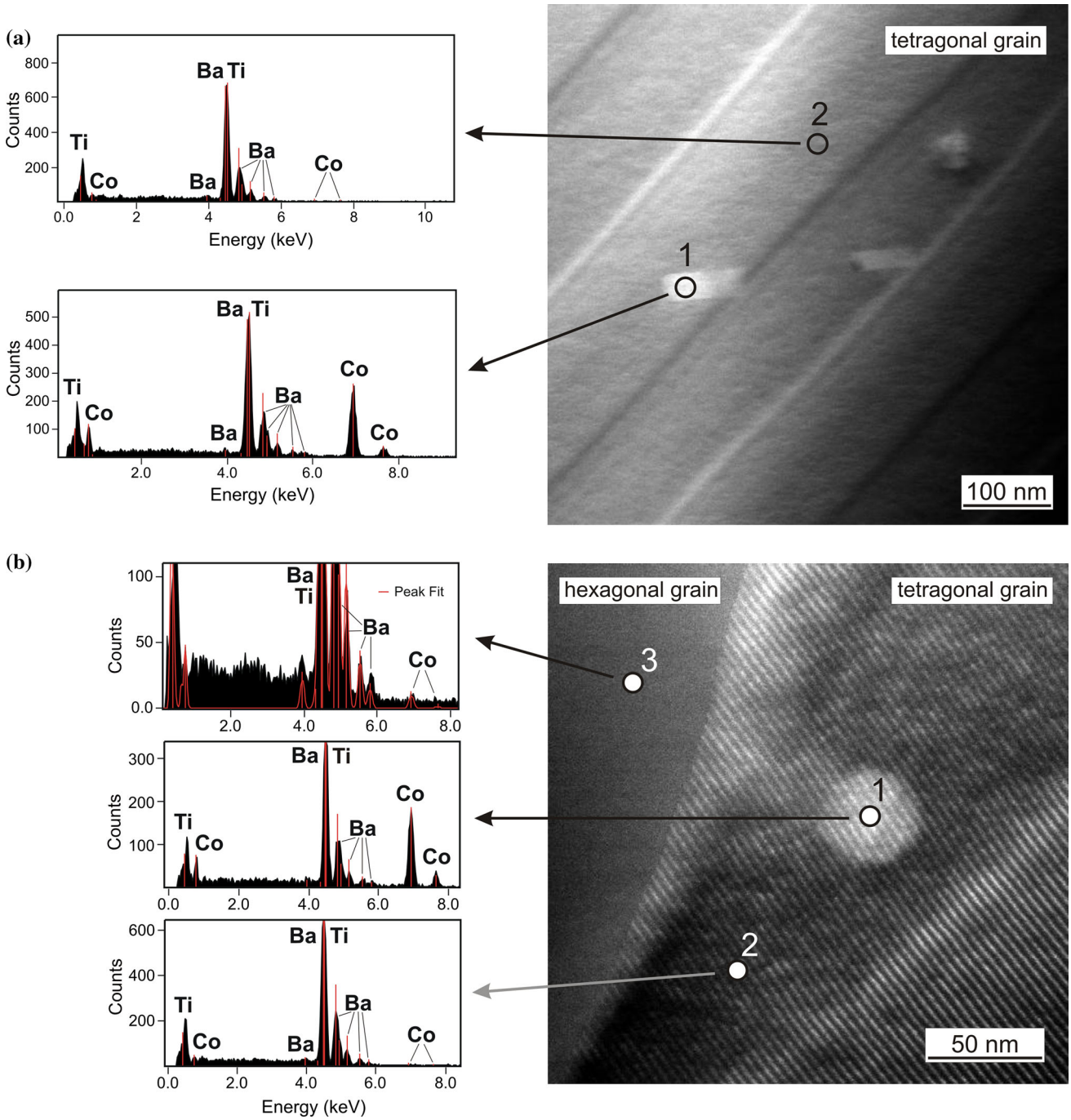

Figure 6 STEM images and EDX spectra at selected points of different regions in Co-doped $BaTiO_3$ ceramics ($x = 0.015$, annealing regime T0). **a** Tetragonal grain. **b** Region between a tetragonal and a hexagonal grain. Measuring points 1, 2, and 3 are explained in the text.

this concentration is near the detection limit, a quantitative measurement for a single measuring point can result in a considerable error. Measurements over an area of 400 × 400 nm^2 reduced this error and resulted in a Co concentration $x = 0.013$, which corresponds very well to the nominal concentration $x = 0.015$ since a part of the weighed Co dopant is precipitated as metallic particles (see Table 1). Obviously, in the grains which maintained the hexagonal phase after the annealing in strongly reducing atmosphere, the Co atoms are still incorporated at Ti sites as isolated paramagnetic impurities [17].

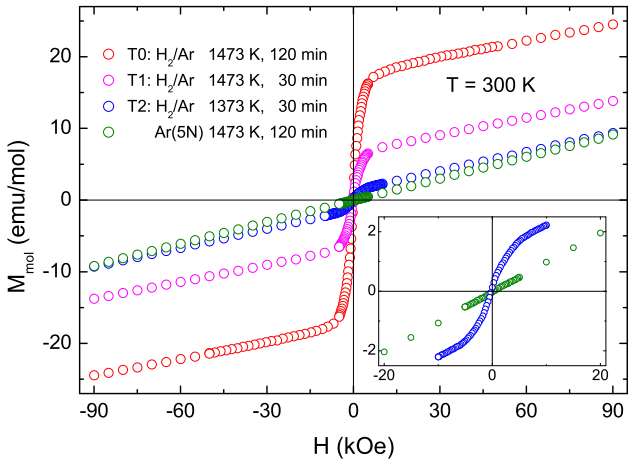

Figure 7 Room-temperature magnetic field dependence of the molar magnetization of Co-doped $BaTiO_3$ ceramics ($x = 0.01$) sintered in air at 1673 K and subsequently subjected to different annealing regimes, T0, T1, and T2 in H_2/Ar stream. The result for a sample annealed in argon stream at 1473 K is shown for comparison.

A careful search for Co precipitations smaller than 10 nm with both electron microscope devices brought no results even with the highest possible resolution of about 0.5 nm. The size of all detected Co particles is at least 20 nm. Hence, the existence of SPM particles in the samples investigated can be excluded. The saturation magnetization of the specimens is exclusively caused by FM Co particles. To investigate the kinetics of the formation of the metallic precipitations, which must be a solid-state diffusion process inside the concerned grains, the temperature schedule of the annealing process was changed. By reduction of annealing time and/or temperature the formation of smaller metallic particles is expected, since the growth of the precipitates is no instantaneous process and the growth velocity should depend on the Co diffusion coefficient in the $BaTiO_3$ matrix. In a first attempt (called regime T1), only the annealing time was reduced from 120 to 30 min compared to the standard annealing regime T0 used for the majority of the samples. For the second attempt (called regime T2), the annealing temperature was reduced from 1473 to 1373 K with a soaking time of 30 min. Figure 7 shows the room-temperature $M_{mol}(H)$ curves of specimens for different annealing regimes with $x = 0.01$ as an example.[3] While the saturation magnetization of sample T1 is reduced to about 50 % of the T0 value, but still exhibiting a distinct saturation effect, the saturation value of sample T2 is rather small compared to its PM contribution at 90 kOe. Besides, its magnetization curve is only slightly different to the exclusively paramagnetic behavior of a sample annealed in pure argon, which is also depicted in Fig. 7. Compared to the annealing regime T0 exhibiting a remanent magnetization of 0.7 emu/mol (see Table 1), the remanence values of the samples annealed under regimes T1 and T2 are decreased to 0.3 and 0.1 emu/mol, respectively, but still indicating FM properties.

Surprisingly, the lower limit of the size distribution of the Co precipitates in the samples subject to annealing regimes T1 and T2 changed only slightly compared to the sample subject to the annealing regime T0. Regarding the occurrence of metallic Co particles, the T1 sample behaves equally to the T0 sample, i.e., the precipitates only occur in tetragonal grains. The particle size distribution is shifted to 20–80 nm reflecting the reduced amount of metallic particles. Despite a very extensive search at highest possible resolution, no Co precipitates were found inside the grains of the T2 sample, but very few Co particles at triple points (Fig. 8a) or at grain boundaries (Fig. 8b). The particle sizes amount to 50 and 17 nm, respectively, excluding SPM properties even for the produced samples with the smallest saturation magnetization.

EPR

Extensive EPR investigations of the PM Co-doped $BaTiO_3$ ceramics were published recently [17]. In air-sintered and in subsequently Ar-annealed hexagonal Co-doped $BaTiO_3$ powder samples, no Co spectra have been observed at room temperature, but only spectra with very low intensities of the impurities Fe^{3+} and Cr^{3+} of the source materials are visible (Fig. 9a). At a temperature lower than 70 K, spectra of two different Co^{2+} centers (Z1 and Z2) were observed. Both centers were assigned to isolated Co^{2+} ions with an effective electron spin $S = ½$. The weakly anisotropic center Z1 ($\bar{g} = 4.33$) was assigned to Co^{2+} ions incorporated at Ti(1) sites in the exclusively corner-sharing oxygen octahedra, whereas the strongly anisotropic center Z2 ($g_{\|c} = 7.29$, $\bar{g}_{\perp c} = 2.18$, c—hexagonal axis) was assigned to Co^{2+} ions incorporated at Ti(2) sites in the trigonally distorted face-

[3] For a qualitative discussion, the chosen Co concentration $x = 0.01$ is sufficiently near the concentration $x = 0.015$ used for the TEM/STEM investigations. .

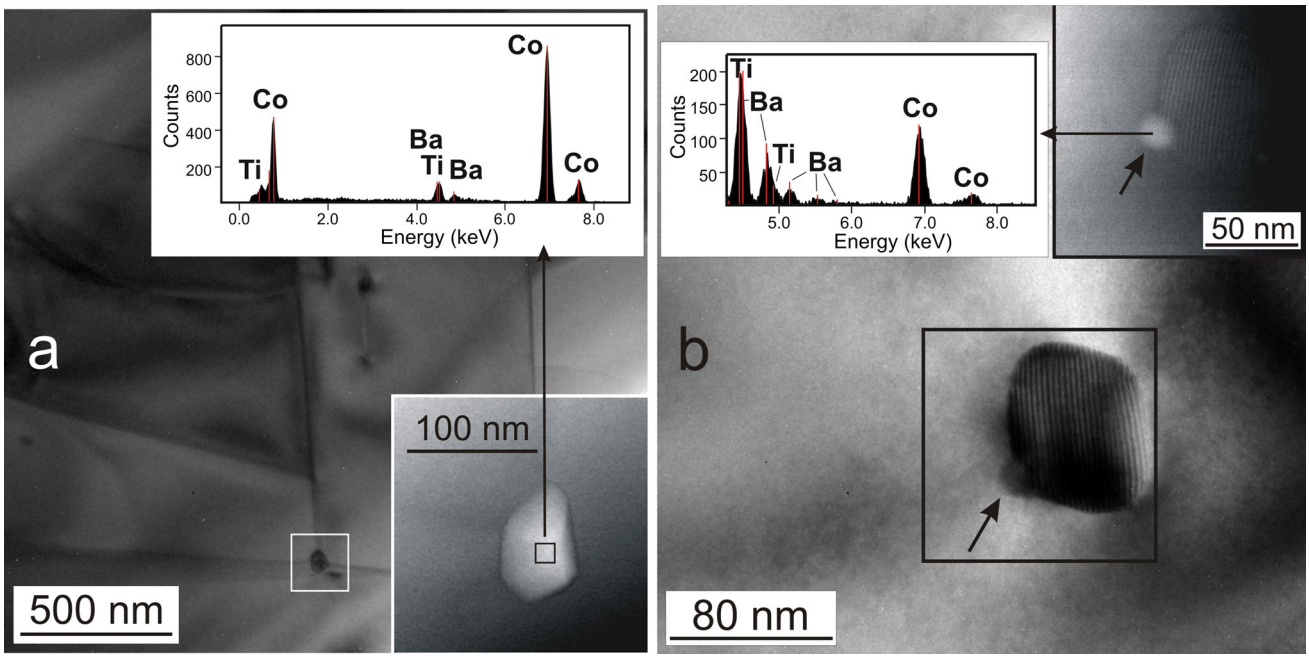

Figure 8 STEM images and EDX spectra of Co precipitations in different regions of Co-doped $BaTiO_3$ ceramics ($x = 0.015$, annealing regime T2). **a** Co precipitation at a triple point. **b** Co precipitations at a grain boundary-enlarged area around the Co particles are shown as *insets*.

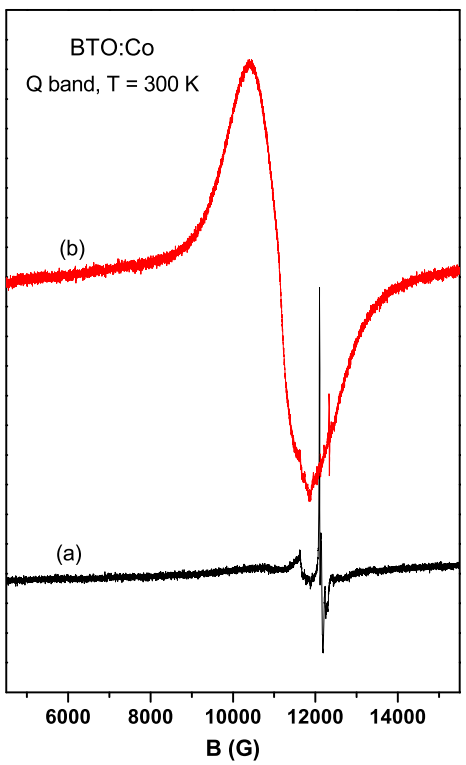

Figure 9 Room-temperature EPR spectrum (Q-band) of Co-doped $BaTiO_3$ powder samples with a Co concentration $x = 0.005$, **a** as-grown and **b** after annealing regime T0.

sharing oxygen octahedra of the hexagonal structure. For the Ar-annealed samples, the intensity ratio of spectra Z1 and Z2 is about 20:1 [17].

After the annealing regime T0 in highly reducing atmosphere, the EPR spectrum of the Co-doped samples has been distinctly changed. Now, in the room-temperature EPR powder pattern, a very intensive line (called spectrum Z3) is observed, see Fig. 9b. Its intensity increases nearly linearly with the Co concentration (Fig. 10). Line width and shape are dependent on microwave frequency and measuring temperature. In the X-band spectrum, the broad line is asymmetric at room temperature, whereas in Q-band experiments, a symmetric shape is measured. Its g factor and line width dependent on the nominal Co concentration are given in Table 2. In contrast to the X-band, these Q-band-measured parameters are nearly temperature independent.

We assign spectrum Z3 with the broad line to the ferromagnetic resonance signal of metallic Co particles precipitated in the tetragonal $BaTiO_3$ grains (see "TEM and EDX" section). Shape and size of these particles are different, and consequently distributions of their structural parameters and their magnetic properties are expected. Since the mean diameter of the Co particles is $d_m \geq 20$ nm most of them are in

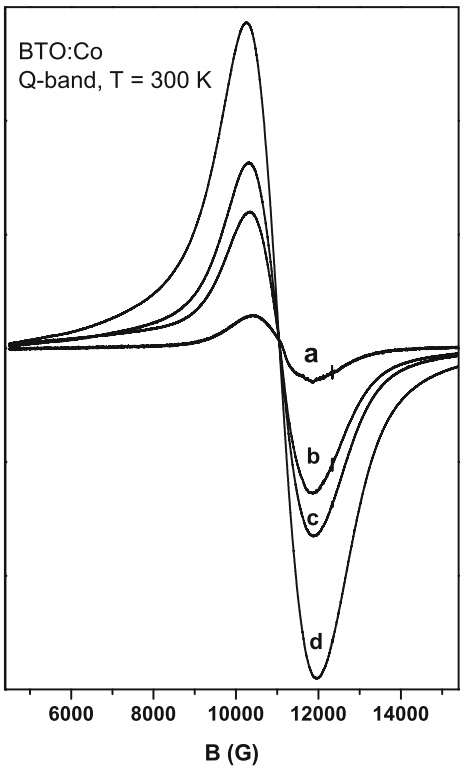

Figure 10 Room-temperature EPR-spectrum (Q-band) of Co-doped $BaTiO_3$ powder samples after applying the annealing regime T0 dependent on the Co concentration. $x = 0.005$ (**a**), 0.010 (**b**), 0.015 (**c**), 0.020 (**d**).

Table 2 g factor and line width values ΔB_{pp} of spectrum Z3 (Q-band) dependent on the nominal Co concentration

x	g factor	ΔB_{pp} (G)
0.005	2.20 ± 0.01	1600 ± 100
0.010	2.20 ± 0.01	1700 ± 100
0.015	2.20 ± 0.01	1950 ± 100
0.020	2.20 ± 0.01	2250 ± 100

the ferromagnetic state. The Larmor precession frequency of the magnetic moment of a particle i in the presence of the effective magnetic field (B^i_{eff}) is

$$\omega^i_{Res} = \gamma B^i_{eff} \quad (2)$$

where γ is the gyro-magnetic ratio, and ω^i_{Res} is the angular frequency. The effective field is the result of the three main components: the external sweeping field B_0, the demagnetizing field B^i_D, and the molecular field B^i_M.[4] The fields B^i_D and B^i_M are dependent on the shape and size of the particle as well as on the orientation of the easy magnetic axis with respect to the external field. The calculation of B^i_{eff} is extremely complicated in our case. Because of the unknown parameters of the particles in our samples, we renounce the detailed interpretation of the ferromagnetic resonance pattern of the metallic Co particles embedded into the $BaTiO_3$ grains.

Fe- and Ni-doped $BaTiO_3$

Since the annealing in strongly reducing atmosphere produces metallic ferromagnetic Co precipitations, it is obviously useful to check this behavior also with iron and nickel as doping elements in $BaTiO_3$. Since the results for Fe- and Ni-doping are qualitatively similar to the Co-doped material, only the nominal concentration $x = 0.02$ for Fe and Ni is presented here as an example. Figure 11 shows the room-temperature $M_{mol}(H)$ curves of Fe-, Ni-, and Co-doped (added for comparison) hexagonal $BaTiO_3$ treated by the highly reducing annealing regime T0. Contrary to the Co-doped samples, no partial retransformation into the tetragonal phase can be observed for Fe- and Ni-doping (at least for $x = 0.02$). The complete hexagonal air-sintered samples remain nearly hexagonal after the annealing regime T0. Also the Fe- and Ni-doped samples exhibit pronounced saturation behavior of the magnetization (after subtraction of the PM contribution) and a distinct magnetic hysteresis (not seen in Fig. 11, H_{coerc} and M_{rem} are

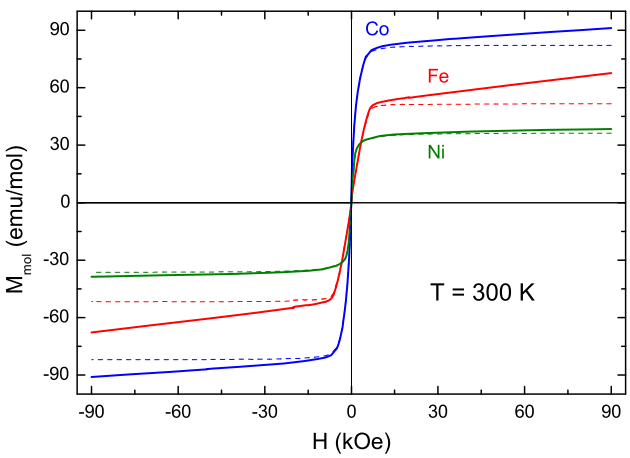

Figure 11 Room-temperature magnetic field dependence of the molar magnetization of Co-, Fe-, and Ni-doped $BaTiO_3$ ceramics sintered in air at 1673 K and subsequently annealed in H_2/Ar stream at 1473 K for a nominal doping concentration of $x = 0.020$.

[4] Here, molecular field means the summarized contributions of magnetic dipole–dipole, exchange, electrostatic multipole, and electron–phonon interactions.

noted in Table 1). Hence, also in the cases of Fe and Ni, the treatment in strongly reducing atmosphere causes remarkable metallic precipitations with a minimum size of 10–20 nm, which explains the FM behavior. The analysis of the $M_{mol}(H)$ curves was carried out as described in "Magnetic measurements" section. The results are also shown in Table 1. The different PM contributions can be roughly explained by the different magnetic moments of the corresponding PM ions. The ions, Fe^{3+} [26], Co^{2+} [17], and Ni^{2+} [27], which are assumed to represent the major impurities, possess in the high-spin ground states total spin values of $S = 5/2$, $3/2$, and 1, respectively. In the rough spin-only approximation (which is a good approximation only for d^5 systems with vanishing total orbital angular momentum like high-spin Fe^{3+}) the effective magnetic moment is $\sim\sqrt{S(S+1)}$. Hence, a decreasing PM contribution in the order Fe > Co > Ni is plausible. Comparing the calculated masses of metallic particles, it is notable that the Fe-doped sample contains the smallest percentage of metallic precipitations. Obviously, most of the weighed Fe remains at Ti sites of the hexagonal $BaTiO_3$ lattice [26] or is incorporated into paramagnetic secondary Ba-Ti-Fe-O phases which cannot be excluded. In contrast, Ni behaves quite differently. More than half of the weighed Ni is found in metallic particles, while for Co, the percentage is about 40 %. These different behaviors could be explained by, e.g., different diffusion coefficients of Fe, Co, and Ni in the $BaTiO_3$ lattice. The three FM doping elements also exhibit different threshold fields H_T to achieve nearly complete alignment of the magnetic dipoles, i.e., the saturation state of magnetization. A coarse estimation of H_T was done by the fit of the $M_{mol}(H)$ curves by the simple arctan function [28].

$$M(H) = \frac{2}{\pi} M_{sat} \arctan\left(\frac{H \pm H_c}{H_T}\right). \quad (3)$$

The determined threshold fields of Fe, Co, and Ni amount to 2460, 1150, and 750 Oe, respectively. Since H_T is somehow correlated to the anisotropy energies of the FM metals, the observed trend is somewhat surprising. The anisotropy energy of the lower-symmetric, hexagonal Co metal is about one order larger than the energies of the cubic Fe and Ni metals [29]. Hence, we expected Co to have the highest threshold field. Moreover, the threshold field also depends on the volume of the FM particles, size distributions of which are unknown for Fe and Ni. Finally, it can be noted that only the magnetization curve of the Ni-doped sample follows the arctan curve very well. Both the other curves significantly deviate from the arctan function in the vicinity of H_T pointing to a distribution of the threshold values of the FM precipitations, which is caused by the nonuniform size distribution of the metallic particles of Co and probably also of Fe.

In the as-prepared samples doped with Fe^{3+} and Ni^{2+} ions, only EPR spectra of the isolated ions incorporated into the host lattice on Ti sites were detected (for details see [3, 4, 26, 30]). No ferromagnetic resonance absorption could be detected by measuring the temperature dependence of the spectra in X- and Q-bands. After the samples were subjected to annealing regime T0, the paramagnetic spectra of isolated ions disappeared, and a very intensive spectrum consisting of a very broad line without any structure at room temperature was observed in X- and Q-bands. The intensity of this line

Table 3 g factor values and line widths of metallic particles in Fe-, Co-, and Ni-doped barium titanates ($x = 0.010$) measured at room temperature

Particle	g factor $f = 34$ GHz	ΔB_{pp} [G] $f = 9.5$ GHz	ΔB_{pp} [G] $f = 34$ GHz
Fe	2.12 ± 0.01	750 ± 60	1200 ± 100
Co	2.20 ± 0.01	950 ± 60	1700 ± 100
Ni	2.19 ± 0.01	650 ± 60	1200 ± 100

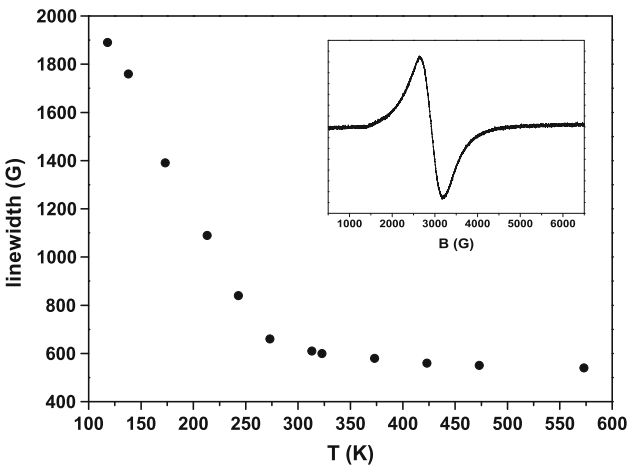

Figure 12 Temperature dependence of the line width of the ferromagnetic resonance signal (X-band) for Ni particles embedded in $BaTiO_3$ ceramics. In the *inset*, the room-temperature spectrum is shown.

is proportional to the concentration of the doping materials. Spectroscopic splitting factor and peak-to-peak line widths ΔB_{pp} measured at 293 K in X- and Q-bands are given in Table 3. With the decreasing temperature, the lines become broader, shifts of the resonance fields to lower magnetic fields are observed, and the line shapes become more asymmetric. Figure 12 shows the temperature dependence of the width ΔB_{pp} of the broad line for Ni-doped samples after the annealing regime T0. The experimentally determined g factor values and room-temperature line widths are characteristic values for ferromagnetic resonance spectra of metallic Fe and Ni nanoparticles in solids.

Summary and conclusion

Hexagonal $BaTiO_3$ ceramics, doped with Fe, Co, or Ni, exhibit a superposition of PM and FM behavior if the air-sintered samples are post-annealed in strongly reducing atmosphere (H_2/Ar stream) at 1473 K. The PM properties originate from isolated Fe^{3+}, Co^{2+}, and Ni^{2+} ions, respectively, which are incorporated at Ti sites of the hexagonal lattice. The FM properties are caused by precipitations of the dopants as metallic particles. Detailed investigations of the Co-doped samples showed that these precipitations exclusively occur in grains (max. 20 %) which are retransformed from the hexagonal 6H- to the 3C-$BaTiO_3$ polytype (tetragonal at room temperature) during the reducing treatment, while in the hexagonal grains, no Co precipitates (detection limit 0.5 nm) can be found. The size distribution of metallic particles in the tetragonal grains amounts to about 15–100 nm, thus excluding partly SPM behavior, since the transition from FM to SPM behavior only occurs for particle sizes well below 10 nm. In very rare cases, metallic precipitations (>15 nm) also occur at grain boundaries or triple points additionally contributing to the FM properties. The Co concentration in the tetragonal grains is below the detection limit of the EDX detector, whereas the Co concentration in the still hexagonal grains corresponds more or less to the nominal Co content of the specimens. Hence, during the reducing treatment, all incorporated Co ions of the retransforming, initially hexagonal grains have to move to the precipitation loci by solid-state diffusion processes forming the final metallic particles inside the grains.

Revisiting our former investigations of hexagonal Mn-doped $BaTiO_3$ where the partial retransformation into 3C-$BaTiO_3$ after annealing in strongly reducing atmosphere was already observed [20], we suppose that also in the case of Mn, the retransformed grains exhibit precipitations of metallic Mn (similar to that reported for Co, Fe, and Ni particles), which were not detected since metallic Mn is not ferromagnetic, and since we did not seek for such Mn precipitations by TEM.

Generalizing our findings, we assume that the annealing in strongly reducing atmosphere of $BaTiO_3$ samples doped with the other 3d dopants like Sc, V, Cr, Cu, and Zn also produces metallic precipitations of the dopants. Regarding the observation of FM behavior of Fe-doped $BaTiO_3$ in the literature [7–16], we can only speculate whether in some cases the FM properties were simply caused by metallic Fe precipitations, at least for samples subjected to a reducing treatment [10, 13, 14]. The annealing in pure oxygen also resulted in certain FM properties [10, 15, 16]. Since those authors applied rather high Fe concentrations between 10 and 30 mol%, a careful search for Fe precipitations by TEM or STEM/EDX should be very useful to exclude metallic particles in the discussion of the magnetic results. Recent studies show also that even very small Fe concentrations «1 mol% in $BaTiO_3$ ceramics can cause weak FM behavior even if the samples were sintered/annealed in air [31].

References

[1] Rabe K, Ahn ChH, Triscone JM (2007) Physics of ferroelectrics: a modern perspective. Springer, Berlin

[2] Kitagawa Y, Hiraoka Y, Honda T, Ishikura T, Nakamura H, Kimura T (2010) Low-field magnetoelectric effect at room temperature. Nat Mater 9:797–802

[3] Possenriede E, Jacobs P, Schirmer OF (1992) Paramagnetic defects in $BaTiO_3$ and their role in light-induced charge transport: I ESR studies. J Phys 4:4719–4742

[4] Possenriede E (1992) Paramagnetische Störstellen in Bariumtitanat und ihre lichtinduzierten Umladungen. Dissertation, University of Osnabrück, Germany

[5] Lee JS, Khim ZG, Park YD, Norton DP, Theodoropoulou NA, Budai JD, Boatner SJ, Pearton SJ, Wilson RG (2003) Magnetic properties of Co- and Mn-implanted $BaTiO_3$, $SrTiO_3$ and $KTaO_3$. Solid State Electron 47:2225–2230

[6] Khalitov NI, Khaibullin RI, Valeev VF, Dulov EN, Ivoilov NG, Tagirov LR, Kazan S, Sale AG, Mikailzade FA (2012) Structural and magnetic studies of Co and Fe implanted $BaTiO_3$ crystals. Nucl Instrum Methods Phys Res B 272:104–107

[7] Maier R, Cohn JL, Neumeier JJ, Bendersky LA (2001) Ferroelectricity and ferrimagnetism in iron-doped $BaTiO_3$. Appl Phys Lett 78:2536–2538

[8] Rajamani A, Dionne GF, Bono D, Ross J (2005) Faraday rotation, ferromagnetism, and optical properties in Fe-doped $BaTiO_3$. J Appl Phys 98:3907

[9] Ramana EV, Yang SM, Jung R, Jung MH, Lee BW, Jung CU (2013) Ferroelectric and magnetic properties of Fe-doped $BaTiO_3$ thin films grown by the pulsed laser deposition. J Appl Phys 113:187219

[10] Lin F, Shi W (2009) Magnetic properties of transition-metal-codoped $BaTiO_3$ systems. J Alloys Compd 475:64–69

[11] Ray S, Mahadevan P, Mandal S, Krishnakumar SR, Kuroda CS, Sasaki T, Taniyama T, Itoh M (2008) High temperature ferromagnetism in single crystalline dilute Fe-doped $BaTiO_3$. Phys Rev B 77:104416

[12] Du G-P, Hu Z-J, Han Q-F, Qin X-M, Shi W-Z (2010) Effects of niobium donor doping on the phase structures and magnetic properties of Fe-doped $BaTiO_3$ ceramics. J Alloys Compd 492:L79–L81

[13] Chakraborty T, Ray S, Itoh M (2011) Defect-induced magnetism: test of dilute magnetism in Fe-doped hexagonal $BaTiO_3$ single crystals. Phys Rev B 83:144407

[14] Chakraborty T, Meneghini C, Aquilanti G, Ray S (2014) Investigating the development of spurious magnetism in single crystalline $BaTi_{0.95}Fe_{0.05}O_{3-\delta}$ with high δ by local structural probes. J Phys: Condens Matter 26:196001

[15] Valant M, Arčon I, Mikulska I, Lisjak D (2013) Cation order–disorder transition in Fe-doped 6h-batio$_3$ for dilute room-temperature ferromagnetism. Chem Mater 25:3544–3550

[16] Zorko A, Pregelj M, Gomilšek M, Jagličić Z, Pajić D, Telling M, Arčon I, Mikulska I, Valant M (2015) Strain-induced extrinsic high-temperature ferromagnetism in the Fe-doped hexagonal barium titanate. Sci Rep 5:7703

[17] Langhammer HT, Böttcher R, Müller T, Walther T, Ebbinghaus SG (2015) Defect properties of cobalt-doped hexagonal barium titanate ceramics. J Phys: Condens Matter 27:295901

[18] Rečnik A, Kolar D (1996) Exaggerated growth of hexagonal barium titanate under reducing sintering conditions. J Am Ceram Soc 79:1015–1018

[19] Kolar D, Kunaver U, Rečnik A (1998) Exaggerated anisotropic grain growth in hexagonal barium titanate ceramics. Phys Status Solidi A 166:219–230

[20] Langhammer HT, Müller T, Felgner K-H, Abicht H-P (2000) Crystal structure and related properties of manganese-doped barium titanate ceramics. J Am Ceram Soc 83:605–611

[21] Langhammer HT, Müller T, Böttcher R, Abicht H-P (2003) Crystal structure and related properties of copper-doped barium titanate ceramics. Solid State Sci 5:965–971

[22] Langhammer HT, Müller T, Böttcher R, Abicht H-P (2008) Structural and optical properties of chromium-doped hexagonal barium titanate ceramics. J Phys: Condens Matter 20:085206

[23] Bean CP, Livingston JD (1959) Superparamagnetism. J Appl Phys 30:120S–129S

[24] O'Handley RC (2000) Modern magnetic materials: principles and applications. Wiley, New York

[25] Wang J-Q, Xiao G (1994) Transition-metal granular solids: microstructure, magnetic properties, and giant magnetoresistance. Phys Rev B 49:3982–3996

[26] Böttcher R, Langhammer HT, Müller T, Abicht H-P (2008) 3C–6H phase transition in $BaTiO_3$ induced by Fe ions: an electron paramagnetic resonance study. J Phys: Condens Matter 20:505209

[27] Langhammer HT, Müller T, Walther T (to be published)

[28] Geiler AL, Harris VG, Vittoria C, Sun NX (2006) A quantitative model for the nonlinear response of fluxgate magnetometers. J Appl Phys 99:08B316.

[29] Blundell S (2001) Magnetism in condensed matter. Oxford University Press, Oxford

[30] Böttcher R, Langhammer HT, Müller T (2011) Paramagnetic resonance study of nickel ions in hexagonal barium titanate. J Phys: Condens Matter 23:115903.

[31] Figueras FG, Amorim CO, Amaral J, Agostinho Moreira J, Tavares PB, Alves E, Amaral VS (2016) Magnetoelectric effect probe through ppm Fe doping in $BaTiO_3$. J Alloys Compd 661:495–500